Self-Organization of C 60 Nanoparticles in Carbon Disulfide Solution

ARTICLE *in* THE JOURNAL OF PHYSICAL CHEMISTRY B · JUNE 2003

Impact Factor: 3.3 · DOI: 10.1021/jp0340717

2 AUTHORS, INCLUDING:

Alok D. Bokare

Pohang University of Science and Technology

33 PUBLICATIONS **453** CITATIONS

SEE PROFILE

Self-Organization of C_{60} Nanoparticles in Carbon Disulfide Solution

Alok D. Bokare and Archita Patnaik*,†

Department of Chemistry, Indian Institute of Technology Madras, Chennai - 600036 India

Received: January 11, 2003; In Final Form: April 1, 2003

C_{60} aggregation in neat CS_2 solvent is reported using positronium (Ps) as a fundamental probe, which maps changes in the local electron density of the microenvironment. Specific interactions of the Ps atom with the surrounding dramatically reveal the onset concentration for stable aggregate formation in this solvent to be 0.06 g/dm^3. Spontaneous formation of stable aggregates in the colloidal range (∼90−125 nm) was observed over a narrow concentration range of 0.06−0.36 g/dm^3, beyond which the clusters broke. Variation of aggregate properties with size (proportional to τ_3 [Ps lifetime] and/or λ_3 [Ps annihilation rate, $1/\tau_3$]) are noteworthy. Ps annihilation characteristics in corroboration with transmission electron microscopy and UV−vis absorption spectroscopy demonstrate the solution phase C_{60} structure to be a spherical fractal aggregate with fractal dimension 1.9 and that the growth mode follows a diffusion-limited cluster aggregation mechanism. At a higher concentration beyond 0.36 g/dm^3, an entropy driven phase change was noticed leading to formation of irregular, but oriented crystalline components.

Introduction

Solid C_{60} is characterized as a soft crystal composed of hard pseudosphere models with a diameter of 7.1 Å, stabilized by the aromatic character of π electrons. By virtue of its rigid well-defined geometry in solution phase, the molecule is exempted from subtle conformational or solvent dependent intramolecular vibrational changes.[1] With a similar magnitude of the specific surface energies of interaction among the C_{60} and the solvent molecules, the fullerene molecules in solution display a trend toward aggregate/cluster formation.[2−9] The latter is correlated with the extraordinary physical and chemical peculiarities of C_{60} in solution with respect to thermodynamic, kinetic, and optical properties. The nonmonotone temperature dependence of solubility[10] and the solvatochromic effect[11,12] are to name a few. A thermodynamic approach to the description of cluster formation in C_{60} solutions was put forward based on the droplet model of a cluster[13] that could explain the concentration and temperature dependence of the diffusion coefficients.

Based on modern approaches to the description of the mechanism of fractal cluster growth, Ying et al.[4] showed a slow aggregation of C_{60} in neat dilute benzene in a concentration range 0.78−1.39 mg/mL at room temperature to be reversible. The DLS intensity indicated the aggregates to be fractals of dimension 2.10, with the aggregation kinetics exhibiting an essentially exponential behavior. The fractal growth of C_{60} aggregates followed a reaction limited cluster aggregation (RLCA) mechanism emphasizing that the mass of aggregates grew with time. Slow C_{60} aggregation in neat toluene over a fairly dilute concentration range 0.18−0.78 g/L has also been studied both experimentally and theoretically[7] at room temperature. The aggregation kinetics described the clusters to be fractals with stable $(C_{60})_N$ clusters of sizes >1.2 nm and aggregation number $N \geq 3$. Nath et al.[8] reported the solvent polarity to play an important role in C_{60} aggregation and that an optimum dielectric constant, $\epsilon \geq 13$ was required for cluster sizes of 250−400 nm. Extensive work on aggregation of C_{60}, C_{70}, and their mixture in a number of solvent mixtures (one of them is a good solvent and the other a poor polar organic solvent) has been reported.[12,14] Recently, Rossitza et al.[5] confirmed stable and durable colloidal dispersions in these systems and established the repulsive electrostatic interactions between the particles (measured from electrophoretic mobility and zeta potential calculations) to be the origin of their stability.

Aggregation of C_{60} in neat solvents is relatively less well characterized. The most recent work of Yevlampieva et al.[9] reports C_{60} aggregation in *N*-methyl pyrrolidone using spectral and electrooptical methods. With a strong emphasis on concentration dependence of aggregation, they reported a complex formation between C_{60} and *N*-methyl pyrrolidone at concentrations $<0.05 \times 10^{-2}$ g/cm^3. In the present paper, the work is aimed at studying the C_{60} aggregation behavior in a neat polar solvent, carbon disulfide (CS_2), over a broad concentration range 0.02−2.16 g/dm^3 using "positronium" (Ps) atom, a bound state of free positron (e^+), and an electron (e^-), as a novel fundamental probe. The basis for employing this technique lies with the fact that the mechanism of Ps atom formation and its subsequent interaction with the medium are highly dependent on the physicochemical properties with locally different electron structure of the environment. Any reorganization in the liquid structure is reflected in abrupt changes in the spectral parameters, e^+/Ps lifetimes, and/or intensities as a function of its composition. Reverse micelles have been studied in sodium AOT/water/isooctane mixtures as a function of AOT concentration, H_2O to AOT mole ratio, and temperature using Ps as a probe.[15] It was concluded that Ps formation occurs primarily in the aqueous part of the micelle, the water aggregates representing efficient traps for the positrons. The Ps formation probability (the intensity component) has been strongly influenced by micelles formed upon aggregation of nonionic surfactants, Triton-X 100, in aqueous medium. The influence of the electrolyte, the nature of the cosurfactant and the solvent on the onset of molecular association, and the structure of the dispersions containing

* To whom correspondence should be addressed. E-mail: archita59@yahoo.com.

† Present address: JSPS Fellow, Department of Materials Technology, Chiba University, Japan.

10.1021/jp0340717 CCC: $25.00
Published on Web 06/03/2003

anionic and cationic surfactants have been extensively studied by Ache et al.[16−19] with Ps annihilation and different associative structures existing within the reverse micellar system. Further, important information has been obtained for *o*-Ps formation probability vs surfactant concentration in the critical micelle concentration range[20,21] and phase transitions in liquid crystals.[22,23]

Along with determining a critical (onset) concentration for instantaneous and stable C_{60} aggregate formation in the yet unattempted neat CS_2 solvent, the present work also establishes the onset concentration at which these clusters break down with further structural reorganization of the medium. The results from the Ps experiments are strongly corroborated with high-resolution transmission electron microscopy (HRTEM) measurements and UV−vis absorption spectroscopy.

Materials and Methods

C_{60} of 99.5+% purity was purchased from MER Corporation, and the purity was confirmed through HPLC and mass spectrometry. Carbon disulfide (analytical grade, SRL Chemicals, India) was freshly distilled and dried over molecular sieves prior to use. C_{60} solutions in the concentration range 0.02−2.16 g/dm^3 were prepared by ultrasonication and degassed to remove the dissolved oxygen. These concentrations were much below the saturation concentration/solubility limit in CS_2 (7.92 g/dm^3 ≈ 7.9 mg/mL). During the acquisition of the spectra, no visible color change in the solutions was observed. Bezmelnitsyn[3] reported that at concentrations 3 orders of magnitude less than the saturation limit (at ∼0.007 g/dm^3) practically no clusters exist in the fullerene solution and it contains only the isolated C_{60} molecules.

Positron Lifetime Spectroscopy. Ps annihilates by emitting γ quanta in 0.125 ns from the *para*-Ps (*p*-Ps) state and in 140 ns from the *ortho*-Ps (*o*-Ps) state. In the condensed phase, owing to the difference in the intrinsic lifetimes, the ortho−para conversion through electron exchange with the medium and spin conversion in the presence of internal or external magnetic field affects the *o*-Ps lifetime, reducing it to ∼1−10 ns in the liquid phase depending on the matrix structure and composition. The *o*-Ps mean lifetime (τ) is the inverse of the Ps annihilation rate (λ) and is given by the overlapping integral of the positron density and the electron density (ρ_{el}) at the site of annihilation, as given below, where r_e is the classical electron radius, Ψ_{e^+} denotes the positron wave function, and c is the velocity of light. Here, R denotes the thickness of the electron layer, where annihilation takes place

$$\frac{1}{\tau} = \lambda = \pi r_e^2 c \int_0^R |\psi_{e^+}|^2 \, \rho_{el} \, d^3r \qquad (1)$$

Positron lifetime spectra were recorded by a fast-fast timing coincidence system consisting of BaF_2 scintillation detectors with a timing resolution of 300 ps fwhm for a Co-60 prompt. The positron source was ∼15 μCi of ^{22}Na−acetate sandwiched and sealed in thin Al foils (2.5 μm thickness). All measurements were performed at room temperature (22 ± 1 °C). The lifetime spectra in our experiments were obtained as a combination of three exponentials as

$$y(t) = N_S \int_{i=1}^{n} \alpha_i \lambda_i I(t) * \exp(-\lambda_i t) \qquad (2)$$

where α_i represents the probability of different annihilation channels and $I(t)$ represents the instrumental resolution function. The asterix (*) sign indicates a convolution of the two terms. The lifetime spectra were resolved into three exponentially decaying components by the PATFIT[24] program. This program contains two fitting programs, POSITRONFIT for the extraction of lifetimes and intensities and RESOLUTION for determining the instrumental resolution function. Both of the programs fit a parametrized model function to a distribution of experimental data points (y_i) obeying Poisson statistics. A least squares criterion is used and the values of the k model parameters b_1, ..., b_k that minimize the equation

$$\Phi \equiv \int_{i=1}^{n} w_i (y_i - f_i(b_1, ..., b_k))^2 \qquad (3)$$

are calculated. Here, n represents the number of data points, $f(b_1, ..., b_k)$ is the model prediction for point number i, and w_i is a fixed weight attached to this point and is equal to $1/\sigma_i^2$, with σ_i^2 being the estimated variance of y_i. An iterative fitting technique is used to estimate the fitting parameters (lifetimes and intensities) and characterize the fitted model function and hence the lifetime spectrum. The *o*-Ps lifetime and intensity are represented as τ_3 and I_3 respectively.

Transmission Electron Microscopy. HRTEM measurements and electron diffraction studies of the solutions were performed using a Philips STEM instrument (model SM12) equipped with a field emission gun operated at 120 kV. Microfilms for TEM studies were prepared by placing a drop of the solution on a carbon coated copper grid, and because of the highly volatile nature of CS_2, the solvent evaporation was instantaneous. Thus, all of the experiments followed natural drying, and the aggregate structure in the solution was replicated on the TEM grid. Samples were then transferred to the microscope in a special vacuum transfer sample holder.

UV−vis Absorption Spectroscopy. Electronic absorption spectra were recorded on a Cary 5E double beam spectrophotometer using a 1 cm path length Infrasil cuvette. About 4 mL of the solution were placed in a 5 mL quartz cell, and the temperature of the solution was kept constant at 22 °C.

Results and Discussion

The Ps formation in liquids occurs by the combination of a thermal positron with one of the quasifree electrons knocked out by the positron during its slowing down process. The interaction of Ps with C_{60} in the solution microenvironment can be represented as a donor−acceptor scheme.

$$2\gamma \xleftarrow{\lambda_p} Ps + C_{60} \underset{k_b}{\overset{k_f}{\leftrightarrows}} [Ps^+ - C_{60}^-] \xrightarrow{\lambda_c} C_{60} + 2\gamma$$

C_{60} as an electron acceptor (electron affinity = 2.5 eV) has a first ionization energy of 7.6 eV for its 3-fold degenerate LUMO (t_{1u}) at −1.042 eV with respect to vacuum 0. This enables the [Ps−C_{60}] complex formation as a result of partial electron transfer from Ps to C_{60}. The presence of a solvent stabilizes the complex to a different degree, depending on the nature of the solvent. k_f and k_b are the forward and backward rate constants, λ_p is the pick-off annihilation rate in pure solvent and λ_c is the annihilation rate from the complex, involving the free, *ortho*-, and *para*-Ps contributions. A qualitative energy level diagram can be seen in Scheme 1, where E_a is circumvented by the high electron affinity of C_{60} and E_b is negligible for annihilation from the complex. The *o*-Ps contribution, λ_3 ($1/\tau_3$) was obtained from the spectral deconvolution of the raw data and was found to vary in a concentration range 0.02−2.16 g/dm^3 (Figure 1), as

$$\lambda_3 = \lambda_P + k[C_{60}] \qquad (4)$$

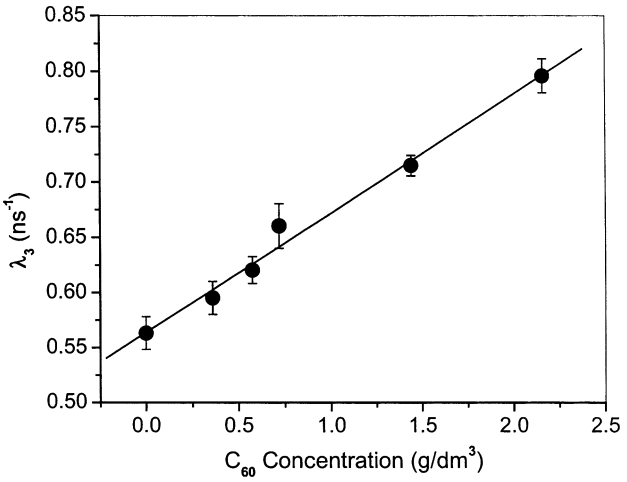

Figure 1. Variation of the *o*-Ps annihilation rate (λ_3) with concentration of the C_{60} solution.

SCHEME 1: Qualitative Energy Level Diagram Depicting the Formation and Annihilation of the Ps−C_{60} Molecular Complex

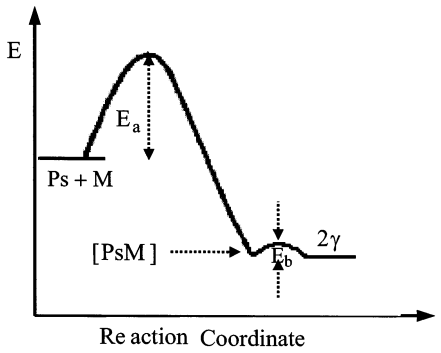

where k is the overall second-order rate constant for the process 1, given by

$$k = (k_f/k_b + \lambda_c)\lambda_c \quad (5)$$

The high value ($\sim 10^{10}$ M^{-1} s^{-1}) of the calculated overall second-order rate constant (k) listed in Table 1 suggests that the annihilation occurs from the [Ps−C_{60}] molecular complex and hence validates the magnitude of λ_3 to be a strong indicative of the solution phase structure of C_{60}. In the case of *o*-Ps pick-off processes, the reaction rate constants are known[25] to be of the order of $\sim 10^8$ M^{-1}s^{-1}.

However, in the lower concentration range from 0.02 to 0.36 g/dm^3, the *o*-Ps annihilation rate (λ_3) follows a completely different trajectory by going through a minimum. Figure 2 represents this behavior. The critical concentration at the minimum of the curve is obtained as 0.06 g/dm^3.

We attribute this critical point to be the onset concentration for stable C_{60} aggregate formation instantaneously upon C_{60} solubilization. At dilute concentrations <0.06 g/dm^3, a decreasing trend in the rate/increasing *o*-Ps lifetime with respect to pure solvent implies a lower magnitude of local electron density around the *o*-Ps, and thus, a probable coexistence of C_{60} monomers and pseudo aggregates of much smaller size is inferred, as will be evident from the TEM experiments in the next section. It has been pointed out[3] that at concentrations 3 orders of magnitude lower than the saturation value clusters practically do not form and isolated fullerene molecules exist in the solution. Beyond $[C]_{critical}$, a sharp enhancement in the rate is representative of the existence of C_{60} clusters in the solution. A close observation of Figure 2 reveals a slope change between 0.06 and 0.36 g/dm^3 and between 0.36 g/dm^3 and beyond concentrations. Beyond 0.36 g/dm^3, because of the increased number density of monomers and the randomly distributed dense C_{60} particles, an increasing electron density annihilates the Ps efficiently, thereby reducing its lifetime. Here, the molecular electrons may screen the e^+e^- Coulomb attraction, resulting in a reduced Ps binding energy, and consequently, a decrease in τ_3 and I_3 at the expense of increasing the free positron intensity (I_2) as was observed in our experiments.

Figure 3 shows the *o*-Ps intensity variation over the concentration range studied. The marked lowering in the *o*-Ps intensity till $[C]_{critical}$ is due to the electron scavenging nature of C_{60} monomer present in this concentration range and has a corresponding match in the annihilation rate profile as shown in Figure 2.

Although C_{60} is nonionic, the interface between the pseudo-aggregated C_{60} spherical clusters/monomers and the surrounding CS_2 solvent (with finite dipole moment) at concentration <0.06 g/dm^3 can be viewed as a charge-polarized interface. The C_{60} components with a greater polarity act as traps for the quasi-free electrons that form in the positron track and inhibit Ps formation. The possibility of such an interpretation is related to the deeper position of the bottom of the conduction band for quasifree electrons in the microphase.[26] Further decrease of I_3 at concentrations >0.36 g/dm^3 may be attributed to an enhanced trapping capability arising from the intrinsic polarity of the islands/unevenly distributed aggregates at such concentrations. The latter can create an attractive atmosphere for the charged entity (e^+) moving in a low viscous solvent, leading to its capture and reduction of the Ps yield. Similar *o*-Ps intensity decrease in Triton−pentanol aggregates upon water addition was attributed to a transition from swollen micelles to a disklike lamellae structure.[27] Thus, the sharp drops in the *o*-Ps intensity component at 0.06 and 0.36 g/dm^3 concentrations due to the self-organization in the system impart a structural rigidity to the solution phase structure of C_{60} and are a sensitive means to determine the onset of aggregation in Fullerene systems. Consequently, the annihilation rate λ_3 cannot be the weighted average of the rates of annihilation of thermalized positrons residing in various environments as found in the direct/reverse micellar systems, but will be the annihilation rate from the [Ps-C_{60}] complex. Hence, unlike in micellar systems, our experimental data show as predominant a change in λ_3/τ_3 as that seen in the I_3 values.

Association in anionic and cationic dispersion systems have been intensely studied using the *ortho*-Ps lifetimes and intensities,[27−30] and it was reported that the formation of the thermalized Ps atom, i.e., the intensity parameter, is greatly reduced when an increasing amount of water becomes solubilized in the reversed micelles formed by sodium bis(2-ethylhexyl) sulfosuccinate in apolar solvents. Similar observations have been made with Triton X-100 surfactant. The application of this technique to potassium oleate−alcohol−oil−water mixture emulsions concluded that a certain water/oil (a long chain aliphatic hydrocarbon, such as hexadecane) ratio is essential for the microemulsion formation. Upon further addition of water, the positron annihilation data sensitively reflected structural rearrangements in these systems, such as the transition from spherical aggregates to disklike lamellae structure. Application of a rigorous diffusion model to a reverse micellar system, sodium AOT/water/isooctane mixtures as a function of AOT concentration[30] implied the *o*-Ps formation to take place

TABLE 1: Solubility of Fullerene C_{60} in CS_2 at Room Temperature and the Associated Solvent Parameters

solvent	solubility (mg/mL)	dielectric constant (ϵ)	viscosity (η) (cP)	k ($M^{-1}s^{-1}$)	$[C_{60}]_{critical}$ (g/dm^3)
carbon disulfide	7.90	2.64	0.36	7.75×10^{10}	0.06

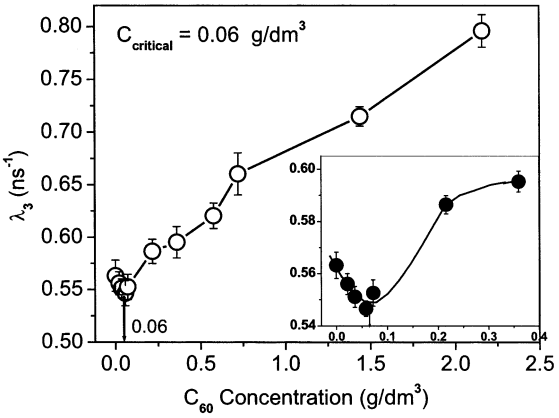

Figure 2. Variation of the *o*-Ps annihilation rate (λ_3) with the C_{60} concentration. The critical concentration for C_{60} aggregate formation, indicated by a minimum λ_3 value, is 0.06 g/dm^3. Inset shows an expanded view of the plot near the critical concentration.

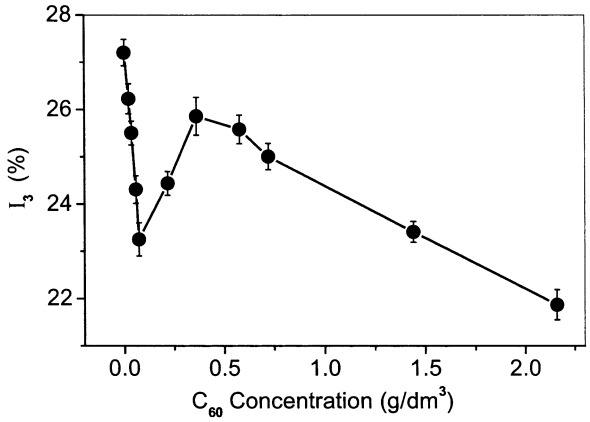

Figure 3. Variation of the *o*-Ps intensity (I_3) with concentration of the C_{60} solution.

in the aqueous part of the micelles, with water aggregates acting as efficient traps.

TEM of C_{60} Fullerene Aggregates in the Concentration Range 0.06−0.36 g/dm^3. The structure of fullerene particles was studied by HRTEM. Figure 4a−f represents the low and high magnification bright field transmission electron micrographs of the aggregates of C_{60} solution in CS_2.

The pictures show spherical clusters appearing in large numbers, and when seen at a higher resolution, their average size is seen to decrease with concentration. Accordingly, at 0.06 g/dm^3 onset concentration, a cluster size of 125 nm is observed as opposed to a cluster size of 90 nm seen at 0.36 g/dm^3 concentration. The structure looks spherical with rodlike tails protruding outward, making possible the attachment of one fullerene molecule with the other. A complete removal of C_{60} molecules from the solution to the aggregate form could not be achieved. Thus, equilibrium exists between them as

$$mC_{60} \overset{K_m}{\longleftrightarrow} (C_{60})_m$$

Also, in the viewed grid region, the cluster size variation is more prominent for the latter i.e., $(C_{60})_m$, in Figure 4f as compared to that for the onset concentration (Figure 4b), where a narrow distribution is observed. As a comparison, the TEM image of the 0.02 g/dm^3 solution (Figure 5) shows a C_{60} monomeric species, whose presence is confirmed from the visible well-arranged unidirectional crystal planes, indicating it to be an isolated single crystal.

The size of the crystallite is 90 nm, and the average center-to-center distance between the fullerene molecules is estimated to be about 0.7 nm. Similar close packing of C_{60} molecules was also observed in the 0.2 nm resolution TEM image of 99.5% C_{60} fullerene powder[31] as well as for crystalline C_{60} grown from a benzene solution.[32]

Electron diffraction of these clusters taken from the same area as the image shows a diffused pattern (Figure 6). The presence of a diffused ring rather than discrete spots suggests that the microdomains within the cluster do not arrange themselves in a crystalline structure pattern and that the clusters are randomly oriented. Amorphous fractal aggregates have been observed previously in inorganic systems such as fumed silica,[33] titania,[34] and aerosols.[35]

Mechanism of C_{60} Cluster Growth. The TEM micrograph of the initial dilute 0.02 g/dm^3 C_{60} solution (Figure 5) shows virtually no difference from that of the C_{60} molecular state. Changes appear with increasing concentration. The appearance of spherical clusters in the concentration range 0.06−0.36 g/dm^3 thus implies an associative mechanism to dominate at high C_{60} concentrations that governs the intermolecular interactions in these solutions. Association of C_{60} to form aggregates in CS_2 solution, its size, and the critical concentration of its formation can be explained in terms of a size-dependent free energy of aggregation; the latter is a cumulative of $C_{60}-C_{60}$ attractive (van der Waals forces) and repulsive electrostatic interactions (electrophoretic mobility measured and ξ-potential calculated for C_{60} colloidal dispersion in acetonitrile-toluene mixture have been found[5] to be -3.30×10^{-4} cm^2/V s and -32.5 mV, respectively). The equilibria between the monomeric C_{60} and its aggregates of variable size $(C_{60})_m$ is associated with a set of equilibrium constants

$$K_m = \frac{[(C_{60})_m]}{[C_{60}]^m}$$

and the free energy of aggregation is equivalent to the free energy of transfer, ΔG_m^0, of a simple C_{60} molecule from monomeric state to aggregate of size (m). Thus, $-RT \ln K_m = m\Delta G_m^0$ where ΔG_m^0 is a function of the environmental variables and the aggregate size. The dependence of the aggregate size on the total C_{60} concentration is closely linked to the size distribution function. Because the size varied in a narrow range (125−90 nm), the size distribution is not very prominent in our TEM images. Nevertheless, the effect of concentration on the size at the critical concentration of aggregation (0.06 g/dm^3) revealed a much steeper size distribution. In micellar environments, at critical micellar concentration, a broader distribution was observed.[36]

The Fractal Concept. A set of points is a fractal if it exhibits self-similarity over all scales. A correlation between their mass and size can be attributed to their fractal structure as $R = \alpha N^{1/D}$ where R is the cluster size, N is the number of primary particles in the aggregate, α is the lacunarity constant, and D is the fractal dimension. Aggregation of colloids, e.g., colloidal polystyrene latex spheres,[37,38] colloidal silica,[39] etc., have served as model

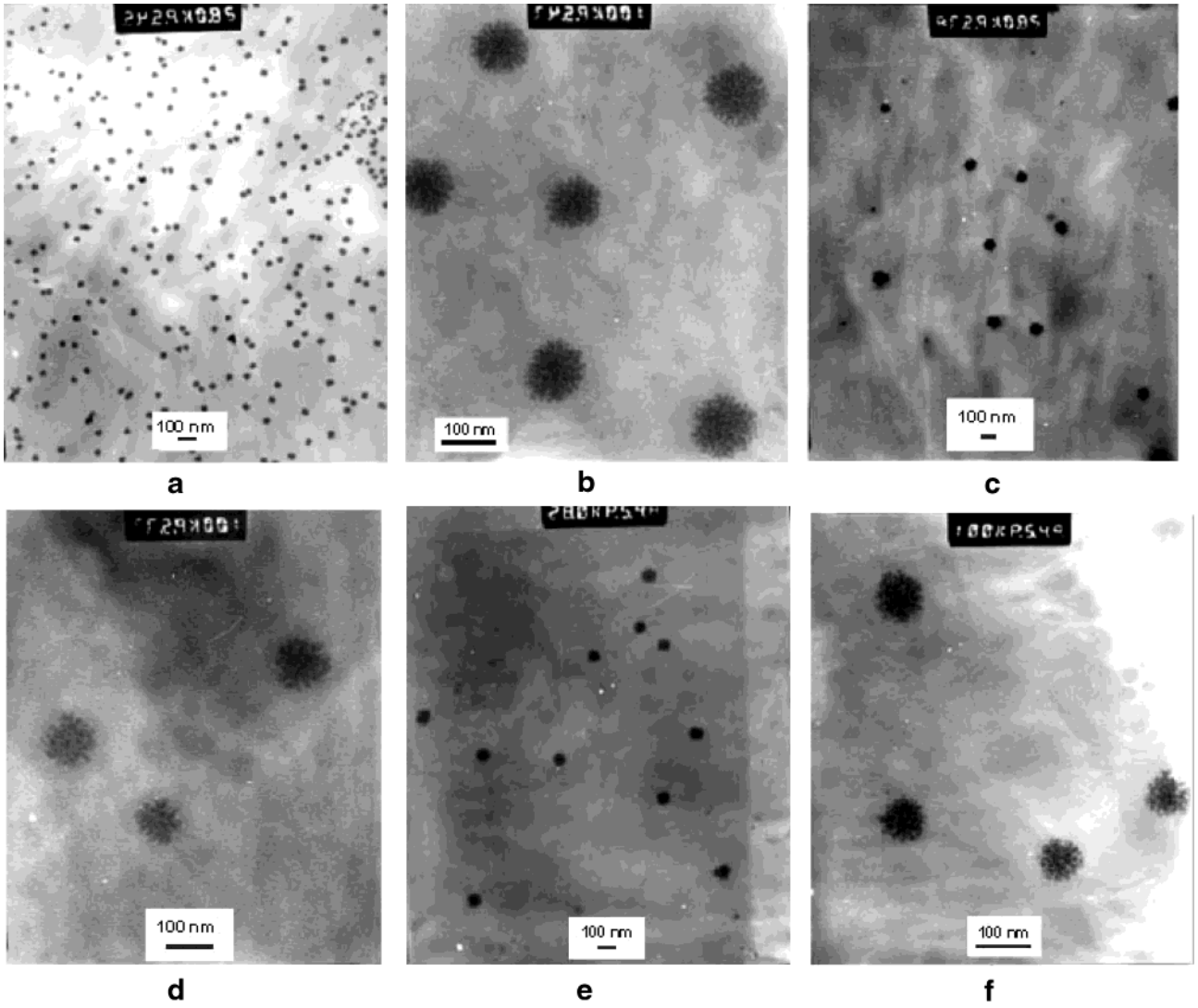

Figure 4. (a) TEM image of the 0.06 g/dm^3 C_{60} solution microfilm. The magnification is 28 000×. (b) TEM image of the 0.06 g/dm^3 C_{60} solution microfilm at a higher magnification (100 000×) showing the microdomains within the spherical aggregate. (c) TEM image of the 0.14 g/dm^3 C_{60} solution microfilm. The magnification is 28 000×. (d) High magnification TEM micrograph of the 0.14 g/dm^3 C_{60} solution microfilm. The cluster size is ∼110 nm. (e) TEM micrograph of the 0.36 g/dm^3 C_{60} solution microfilm at 28 000× magnification. (f) TEM micrograph of the 0.36 g/dm^3 C_{60} solution microfilm at 100 000× magnification.

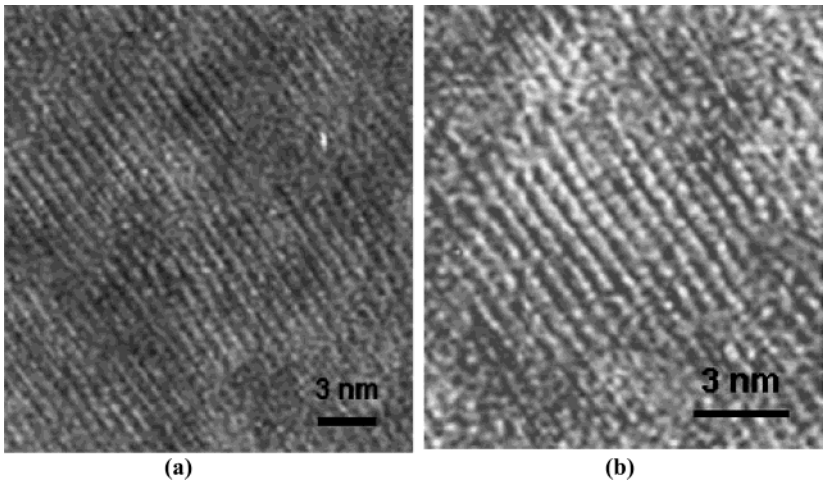

Figure 5. HRTEM images of a fullerene monomer in the 0.02 g/dm^3 C_{60} solution microfilm. Panels a and b show different portions of the same particle.

systems with the use of the fractal concept. The two limiting regions of irreversible colloids, namely, the reaction limited cluster aggregation (RLCA) and the diffusion-limited cluster aggregation (DLCA), have been used to arrive at the structure and kinetics of these aggregates. The former is a slow aggregation process and is dependent on the time taken for particles to

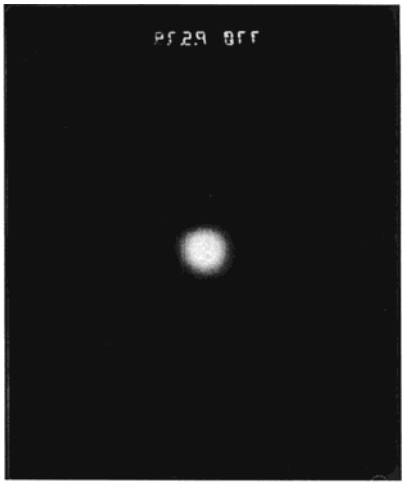

Figure 6. Microdiffraction pattern of the C_{60} cluster at a concentration 0.06 g/dm^3.

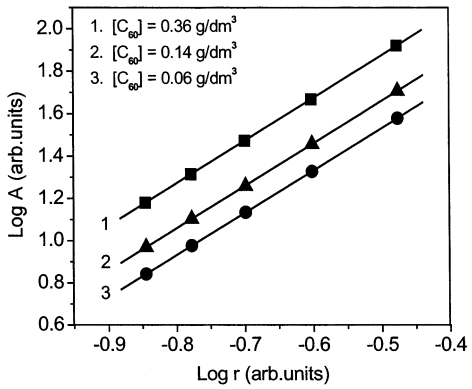

Figure 7. Determination of the fractal dimension of C_{60} cluster aggregates from log(A) vs log(r) plots. Aggregation of clusters is a result of attachment of clusters of comparable sizes (independent of cluster size). (1) $Y = 2.877 + 1.910X$, $D = 1.9$; (2) $Y = 2.662 + 1.898X$, $D = 1.9$; (3) $Y = 2.53 + 1.905X$, $D = 1.9$.

overcome a repulsive energy barrier by thermal activation. The fractal dimension in this case has been found to be 2.1 and the kinetics followed an exponential behavior. In the DLCA model, aggregation is a fast process and is limited by the time taken for the particles to encounter each other by diffusion, and the fractal dimension has been obtained as 1.8. The very first computer simulation for growth of aggregates through diffusion-limited random walk of primary particles was put forward by P. Meakin[40] with a fractal dimension $D = 2.5$.

As observed in the previous section, for the instantaneously formed mass-clusters at and beyond the $[C]_{critical}$, we estimated the fractal dimension adopting the Hausdorf box counting method as

$$D = \lim_{h\to 0} \frac{\log N(h)}{\log\left(\frac{1}{h}\right)} \approx \frac{\log A}{\log r} \qquad (6)$$

where A is the area coverage of the cluster aggregate and r is the radius of gyration. Figure 7 shows the linear plots with $D = 1.9$ over the concentration range for stable cluster formation.

Although the magnitude is higher than the general value of 1.8, owing to a similar size of the clusters as seen in Figure 4b,d,f and the observed fast aggregation, we attribute the growth process to be governed by DLCA. Fractal dimensions for colloidal dispersions of fluorinated polymer particles, studied by small angle neutron scattering, have been found to be 1.9 in the framework of DLCA.[41] Mass fractal structures proposed for organic pigments studied by SAXS have been associated with $D = 2.5$, discussed under RLCA.[42] Under the DLCA model, electrodeposited polypyrrole aggregates have been attributed with $D = 2.5$. When variability of the diffusion coefficient with particle size and transport regime were considered in more complicated simulations, Mountain[43] found fractal dimensions of 1.89 to 2.07 for DLCA. Das et al.[44] reported $D = 1.3$ for N^+ beam induced formation of graphitic clusters through DLCA in poly(*p*-phenylene oxide) matrix. Variation in the D value is thus visualized depending on the embedding dimension and the statistical nature of the structure of a cluster. Koylu et al.[45] reported $D = 1.82$ for soot aggregates from a variety of fuels such as acetylene, propylene, etc., numerically simulated through cluster−cluster aggregation as well as for measured ones through TEM.

TABLE 2: Characteristics of C_{60} Fractal Cluster Aggregates

$[C_{60}]$ in CS_2 (g/dm^3)	0.06	0.14	0.36
C_{60} cluster size (nm)	125	110	90
aggregation number	3.2×10^4	2.5×10^4	1.7×10^4

Kinetics and growth of fractal clusters of C_{60} in solution has been analyzed by Bezmelnitsyn[3] based on the above models. Describing the Brownian motion of two particle aggregates (of comparable size) during their coalescence with Stokes−Einstein and Smoluchowsky's theories, the rate constant (k) for coalescence was calculated to be 10^{-12} cm^3/s, with the saturated concentration of fullerenes, $N_0 \sim 10^{18}$ cm^{-3} at room temperature. Under the diffusion approach, this rate corresponds to a time of attachment process (τ) $\sim (N_0k)^{-1} \sim 10^{-6}$ s, valid for the equilibrium size distribution of clusters. This implies that the growth of C_{60} fractal clusters in solution is instantaneous. A simple calculation will justify a similar conclusion from our experiments. DLCA states

$$R = r_0(N_0kt)^{1/D} \qquad (7)$$

with R as the cluster radius, r_0 as the radius of a C_{60} molecule, and D as the fractal dimension. For the present experimental concentrations, 2 orders of magnitude lower than the saturated one, the time of coalescence of two clusters turns out to be ~3.2 s, thus, justifying the cluster growth to follow DLCA. The aggregation number (n) for the fractal clusters at different concentrations was calculated according to, $n = (R/r_0)^D$, and the values are listed in Table 2.

However, Ying et al.[4] showed a slow aggregation of C_{60} in neat dilute benzene over a period of 100 days with a fractal dimension of 2.10, attributed to RLCA as the growth mode. Slow C_{60} aggregation in neat toluene over a dilute concentration range showed[7] stable $(C_{60})_N$ clusters of sizes >1.2 nm and aggregation number $N \geq 3$ with a maximum at $N = 55$. In their calculation, the polarization interaction of C_{60} aggregates with toluene medium was neglected, which is unlikely in CS_2 medium, which is associated with a finite dipole moment. This effect was further confirmed with the drastic variation in *o*-Ps intensity component as a function of C_{60} concentration.

Concentration Range >0.36 g/dm^3. At concentrations >0.36 g/dm^3 (cf. parts a and b of Figure 8), the clusters further agglomerate to give looser flowerlike structures with an open hole in the center, upon further addition of single C_{60} molecules. Also observed are the fused open-clusters with hollow cores of size varying between 350 and 460 nm. Although inhomogeneously distributed, the molecular aggregates are held together via weak van der Waals forces when dispersed in the solution.

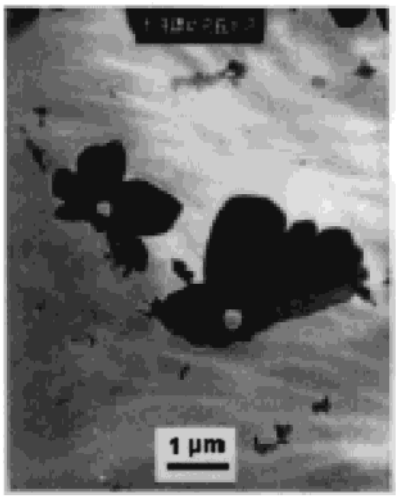

a

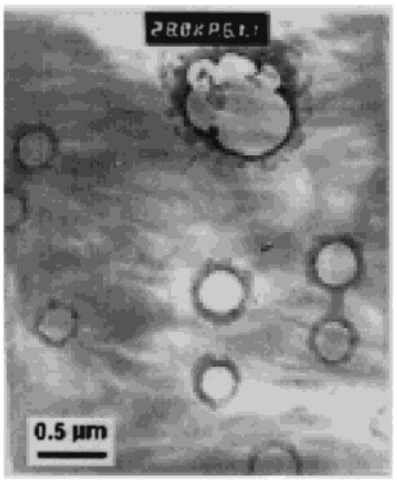

b

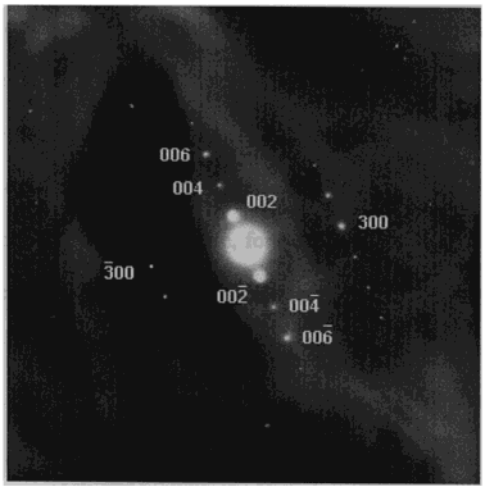

c

Figure 8. (a) TEM micrograph of the 2.16 g/dm^3 C_{60} solution microfilm depicting the presence of agglomerated flowerlike structures with an open hole in the center. (b) TEM image of the 2.16 g/dm^3 C_{60} solution microfilm showing formation of fused open-clusters with hollow cores. (c) Microdiffraction pattern of the agglomerated flowerlike cluster in the 2.16 g/dm^3 C_{60} solution microfilm.

This further unanticipated complexity in the micro-phase/structure reorganization/phase separation is accompanied by an increase in the *o*-Ps annihilation rate seen in Figure 2 (decrease of *o*-Ps lifetime), and we attribute this to a phase transition of the system. These transitions have analogous counterparts in colloidal solutions where the most commonly observed phase transition is solidification with formation of a condensed phase with regular crystal structure, formed upon a change in the external condition.[46] Figure 8c shows the electron diffraction pattern of one of the flowerlike structures to be highly oriented with discrete diffraction spots. The structural anisotropy may be accompanied by the long-range interactions playing a significant role. Structural analysis resembled the hexagonal close packing (hcp) lattice structure, analogous to that shown by C_{60} fullerites grown from a benzene solution.[47]

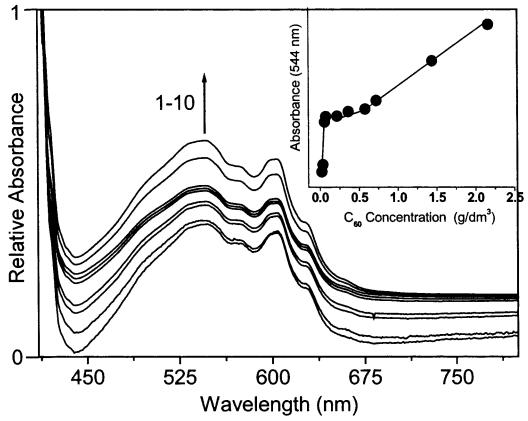

Figure 9. Optical absorption spectra of C_{60} in CS_2 at different concentrations, (1) 0.02, (2) 0.04, (3) 0.06, (4) 0.07, (5) 0.2, (6) 0.36, (7) 0.6, (8) 0.72, (9) 1.44, and (10) 2.16 g/dm^3. All of the spectra are plotted after normalization to the highest concentration of C_{60} used. Spectra for the 0.07 and 0.2 g/dm^3 concentration are coincident. Inset shows the Lambert−Beer (LB) plot for the absorbance versus the C_{60} concentration.

We explain this phase behavior at concentrations >0.36 g/dm^3 to be entropically driven by steric repulsion between the particles, complying with the fact that they are negatively charged.[5] Entropy maximization occurs by minimizing free energy $G = U - TS$ with U, the internal energy = 0 for hard and impenetrable particles.[48] Entropically driven microphase transitions in mixtures of colloidal rods and spheres have been discussed where it is assumed that attractive interactions are necessary to generate phases with long range order.[49] The physical origin of the phase separation may be explained as follows: When the components phase separate, the free volume of the suspension is maximized which precedes the raising of the translational entropy of the molecules at the expense of lowering the entropy of mixing. At low concentrations, entropy mixing dominates and the solution is miscible. However, at high concentration, with gain in free volume, phase separation occurs with a repulsive interparticle potential.

UV−vis Absorption Spectroscopy. From the optical absorption measurements of C_{60} in different aromatic solvents of varying dielectric constants (ϵ), it has been reported that the absorption characteristics do not change with concentration and the absorbance follows the Lambert−Beer (LB) relation[50] for solvents such as benzene and toluene. In polar aromatic solvents such as benzyl alcohol and benzonitrile, however, the C_{60} solutions show different absorption spectra as the fullerene concentration is increased,[8] and these changes are attributed to the formation of C_{60} aggregates beyond a certain critical concentration. In the present work, ground-state absorption spectra of C_{60} in polar CS_2 over the concentration range 0.02−2.16 g/dm^3 have been recorded. Figure 9 shows the absorption

spectra, plotted after normalization to the highest C_{60} concentration (2.16 g/dm^3) used.

As the C_{60} concentration increases, the spectral characteristics change with a minor blue shift in the 544 nm absorption peak but with an enhancement in the relative absorbance and a decrease in the depth of the 440 nm valley. The inset of Figure 9 shows the LB plot at 544 nm, indicating breaks at 0.06 and at 0.6 g/dm^3 and, hence, the changes in the molecular form at these concentrations in CS_2. This situation matches excellently with the results obtained from the positron annihilation lifetime (PAL) and TEM measurements, wherein, 0.06 g/dm^3 concentration was the onset concentration for cluster formation and at concentrations beyond 0.6 g/dm^3 the formation of agglomerated flowerlike patterns was observed.

Conclusion

The basic difference in the concentration dependent C_{60} structure in CS_2 solvent commands the existence of several competing mechanisms during solubilization and an increasing interaction between C_{60} molecules results in a displacement of equilibrium toward the solid state**.** At middle concentrations, just at or after the onset of aggregation, the clusters may be highly immobilized owing to strong intermolecular interactions. On attaining the full size and after that at a larger concentration, the rigidity of the cluster core is greatly reduced and the properties of the cluster approach that of bulk, accompanied by a phase separation. At dilute concentrations, before the critical point, the system may remain as an isotropic liquid with C_{60} monomers and monomers tending to aggregate but cannot because of instability or nonattainment of an equilibrium state owing to low concentration, accompanied by large solute−solvent interactions. These results were obtained from a microscopic picture of the surroundings of Ps in the C_{60} solution and TEM and supported by optical absorption studies.

Acknowledgment. This work has been supported by the Department of Science and Technology (DST), Government of India, Grant No. SP/S1/H-33/95. A.D.B. thanks the DST, Govt. of India, for a Research Fellowship.

References and Notes

(1) Castillo, R.; Garza, C.; Ramos, S. *J. Phys. Chem.* **1994**, *98*, 4188−4190.
(2) Ying, Q.; Marecek, J.; Chu, B. *J. Chem. Phys.* **1994**, *101* (4), 2665.
(3) Bezmel'nitsyn, V. N.; Eletskii, A. V.; Stepanov, E. V. J. *J. Phys. Chem.* **1994**, *98*, 6665.
(4) Ying, Q.; Marecek, J.; Chu, B. *Chem. Phys. Lett.* **1994**, *219*, 214.
(5) Alargova, R. G.; Deluchi, S.; Tsujii, K. *J. Am. Chem. Soc.* **2001**, *123*, 10460−10467.
(6) Nath, S.; Pal, H.; Palit, D. K.; Sapre, A. V.; Mittal, J. P. *J. Phys. Chem B* **1998**, *102*, 10158−10164.
(7) Bulavin, L. A.; Adamenko, I. I.; Yashchuk, V. M.; Ogul'chansky, T. Yu.; Prylutskyy, Yu. I.; Durov, S. S.; Scarff, P. *J. Mol. Liq.* **2001**, *93*, 187−191.
(8) Nath, S.; Pal, H.; Sapre, A. V. *Chem. Phys. Lett.* **2000**, *327*, 143−148.
(9) Yevlampieva, N. P.; Birulin, Y. F.; Melenevskaja, E. V.; Zgonnik, V. N.; Rjumtsev, E. I. *Colloids Surf. A* **2002**, *209* (2−3), 167−171.
(10) Ruoff, R. S.; Malhotra, R.; Huestis, D. L. *Nature* **1993**, *361*, 140.
(11) Sun, Y.-P.; Bunker, C. E. *Nature* **1993**, *365*, 398.
(12) Ghosh, H. N.; Sapre, A. V.; Mittal, J. P. *J. Phys. Chem.* **1996**, *100*, 9439.
(13) Bezmel'nitsyn, V. N.; Eletskii, A. V.; Stepanov, E. V. J. In *Progress in Fullerene Research*; Kuzmany, H., Ed.; World Scientific: Singapore, 1994; p 45.
(14) Ahn, J. S.; Suzuki, K.; Iwasa, Y.; Otsuka, N.; Mitani, T. *J. Lumin.* **1998**, *76/77*, 201.
(15) Marques, M. F. F.; Burrows, H. D.; Miguel, M. D.; Lima, A. P.; Gil, C. L.; Duplatre, G. *J. Phys. Chem.* **1996**, *100*, 7595−7602.
(16) Boussaha, A.; Djermouni, B.; Fucugauchi, L. A.; Ache, H. J. *J. Am. Chem. Soc.* **1980**, *102*, 4654−4658.
(17) Boussaha, A.; Ache, H. J. *J. Phys. Chem.* **1981**, *85*, 1693−1697.
(18) Jean, Y. C.; Ache, H. J. *J. Am. Chem. Soc.* **1977**, *99*, 7504.
(19) Jean, Y. C.; Ache, H. J. *J. Phys. Chem.* **1978**, *82*, 811.
(20) Ache, H. J. In *Positron Annihilation*; Coleman, P. G., Sharma, S. C., Diana, L. M., Eds.; North-Holland: Amsterdam, 1982; p 773.
(21) Jean, Y. C.; Ache, H. J. *J. Am. Chem. Soc.* **1979**, *100*, 984.
(22) Jean, Y. C.; Hancock, A. J. *J. Chem. Phys.* **1982**, *77*, 5836.
(23) Bokare, A. D.; Das, D.; Amenitsch, H.; Patnaik, A. *Solid State Commun.* **2002**, *122* (6), 329−333.
(24) Kirkegaard, P.; Pedersen, N. J.; Eldrup, E. *PATFIT-88* (Riso-M-2740).
(25) Bokare, A. D.; Patnaik, A. Unpublished work.
(26) Grafutin, V. I.; Prokopev, E. P. *Phys.-Uspekhi* **2002**, *45* (1), 59−74.
(27) Boussaha, A.; Djermouni, B.; Fucugauchi, L. A.; Ache, H. J. *J. Am. Chem. Soc.* **1980**, *102*, 4654−4658.
(28) Boussaha, A.; Ache, H. J. *J. Phys. Chem.* **1981**, *85*, 1683−1697.
(29) Das, S. K.; Ganguly, B. N. *J. Radioanal. Nucl. Chem.* **1998**, *230* (1−2), 17−20.
(30) Marques, M. F. F.; Burrows, H. D.; Miguel, M. G.; Lima, A. P.; Gil, C. L.; Duplatre, G. *J. Phys. Chem.* **1996**, *100*, 7595−7602.
(31) Voronov, O. A.; Tompa, G. S.; Kcar, B. H.; Mayo, W. E.; Liao, S.-C.; Sadangi, R. K.; Livi, K. J.; Loutfy, R. O. *Report DMI-41023-Final for US Army Aviation and Missile Command*, Department of Defense (DoD), Defense Advanced Research Projects Agency, 1998; p 58.
(32) Saito, Y.; Suzuki, N.; Shinohara, H.; Hayashi, T.; Tomita, M. *Ultramicroscopy* **1992**, *41*, 1−9.
(33) Forsman, J.; Harrison, J. P.; Rutenberg, A. C*an. J. Phys.* **1987**, *65*, 767.
(34) Lee, J. H.; Beaucage, G.; Pratsinis, S. E.; Vemury, S. *Langmuir* **1998**, *14*, 5751.
(35) Sorensen, C. M. *Aerosol Sci. Technol.* **2001**, *35* (2), 648.
(36) Mukherjee, P. *J. Phys. Chem.* **1972**, *76*, 565.
(37) Cametti, C.; Codastefano, P.; Tartaglia, P. *Phys. Rev. A* **1987**, *36*, 4916.
(38) Zhou, Z.; Chu, B. *J. Colloid Interface Sci.* **1991**, *143*, 356.
(39) Martin, J. E. *Phys. Rev.* **1987**, *36*, 3415.
(40) Meakin, P. *Phys. Rev. A* **1983**, *27*, 2616.
(41) Lattuada, M.; Wu, H.; Morbidelli, M. *Phys. Rev. E* **2001**, *64*, 61404.
(42) Lee, J. H.; Beaucagl, G.; Pratsinis, S. E.; Vemury, S. *Langmuir* **1998**, *14*, 5751.
(43) Mountain, R. D.; Mulholland, G. W. *Langmuir* **1988**, *4*, 1321−26.
(44) Das, A.; Dhara, S.; Patnaik, A. *Phys. Rev. B* **1999**, *59*, 11069−11076.
(45) Koylu, U. O.; Faeth, G. M.; Farias, T. L.; Carvalho, M. G. *Combust. Flame* **1995**, *100*, 621−633.
(46) Asherie, N.; Lomakin, A.; Benedek, G. B. *Phys. Rev. Lett.* **1996**, *77*, 4832.
(47) Takata, M.; Kubota, Y.; Sakata, M.; Harada, J.; Saito, H.; Shinohara, H.; Nagashima, H.; Ando, Y. *Presented at the Autumn Meeting (46th NENKAI) of the Physical Society of Japan*, University of Hokkaido, 1991.
(48) Forsyth, P. A., Jr.; Marcedja, S.; Mitchell, D. J.; Ninham, B. W. *Adv. Colloid Interface Sci.* **1978**, *9*, 37−60.
(49) Adams, M.; Dogic, Z.; Keller, S. L.; Fraden, S. *Nature* **1998**, *393*, 349.
(50) Birks, J. B. *Photophysics of Aromatic Molecules*; Wiley: London, 1970.